No. 674 May 2024

Simulation techniques for the viscoelastic fluids with pure polymer melts based on EVSS approach

R. Ahmad, P. Zajac, S.Turek

ISSN: 2190-1767

Simulation techniques for the viscoelastic fluids with pure polymer melts based on EVSS approach

R. Ahmad, P. Zajac and S. Turek

Institute for Applied Mathematics, LS III, TU Dortmund University,
Vogelpothsweg 87, 44227 Dortmund, Germany
rida.ahmad@math.tu-dortmund.de
peter.zajac@math.tu-dortmund.de
stefan.turek@math.tu-dortmund.de

Key Words: Elastic Viscous Stress Splitting, Viscoelastic fluids, Pure polymer melts, Finite Element Method, Decoupled and monolithic approaches, Shear thinning effect

ABSTRACT

To obtain the solution of the viscoelastic fluid simulation with pure polymer melts is a highly challenging task due to the lack of the solvent contribution to the viscosity in the standard viscoelastic formulation. The aim of this paper is to present a mixed finite element method for solving the three field Stokes flow with zero solvent viscosity employing the Elastic Viscous Stress Splitting (EVSS) formulation. On one hand, the EVSS formulation helps to recover the velocity coupling back into the momentum equation by the application of the change of variables in the standard viscoelastic formulation. On the other hand, additional terms containing the second order velocity derivatives appear in the convective part of the constitutive equation for stress. We have reformulated the convective term by considering the divergence-free nature of the velocity field and shifted the higher order derivatives to the test function in the weak formulation. The velocity, pressure and stress are discretized by the higher order stable FEM triplet $Q_2/P_1^{disc}/Q_3$. The proposed scheme is tested for Oldroyd-B, Giesekus and PTT exponential fluids employing both the decoupled and the monolithic solution approaches. The numerical results are obtained on four to one contraction for highly viscoelastic fluids with the aim to observe the shear-thinning effect as the relaxation parameter increases.

1 Introduction

Viscoelastic fluids are complex fluids that exhibit both viscous and elastic behavior. Depending upon the stress such fluids either behave as solid or liquid. The numerical simulation of viscoelastic fluids is an important subject which has numerous applications in the design of polymer materials. Even after several decades of research, the simulation of such flows is still a challenging and costly task. Hence, the development of efficient numerical methods for computing fluid flow problems is a major issue. Furthermore, the involved difficulties are amplified in case of simulating applications from the rubber industry, where specific types of viscoelastic materials are processed, in detail pure polymer melts, i.e. with vanishing solvent contribution to the viscosity. Thus, the corresponding diffusive operator vanishes from the momentum equation of the Stokes problem, which causes several difficulties regarding discretisation and solution techniques of the underlying three-field formulation. On the one hand, an additional stability condition regarding the choice of the approximating spaces with respect to the velocity and stress variables needs to be taken into account besides the usual velocity-pressure coupling. On the other hand, there are constraints regarding the implemention of the decoupled schemes. The decoupled approach is beneficial in a sense that,

the velocity and pressure computation is decoupled from the stress computation in each iteration, thus reducing memory requirements and possibly CPU time. In this paper, the utilization of an Elastic Viscous Stress Splitting (EVSS) approach to simulate viscoelastic fluid flows is pursued, aiming to address the aforementioned issues. The EVSS formulation is one way to reintroduce velocity coupling into the momentum equation involving utilization of a change of variables initially proposed for second-order fluids by Perera and Walters [1], and Mendelson et al. [2] for the flow of second order fluids and later extended to viscoelastic flows by Beris et al. [3, 4]. The EVSS formulation is obtained by splitting of the extra-stress tensor $\boldsymbol{S}$ into the viscous and elastic parts. The splitting is performed as follows:

$$\boldsymbol{S} = 2\eta_p \mathbf{D}(\mathbf{u}) + \mathbf{E} \tag{1}$$

The introduction of the splitting leads to the change of variables in the momentum and constitutive equation yielding a set of equations involving the velocity $\mathbf{u}$, pressure p, and the new variable $\boldsymbol{E}$. From one perspective, the velocity coupling is recovered back into the momentum equation thus providing the opportunity to treat the formulation in a decoupled/operator splitting way. However, new terms appear in the constitutive equation for stress. Second order velocity derivatives, which are very challenging to handle computationally, are involved in the convected derivative of the rate of deformation tensor in the constitutive equation. Rajagopalan et al. [5] proposed the introduction of the rate of deformation tensor as an unknown, leading to a rather versatile class of EVSS methods. Thereafter, a sequence of papers followed which outlined analysis of the method as well as numerical experiments [6, 7, 8, 9, 10]. The treatment of the deformation tensor as a distinct variable increases the problem size which in turn requires higher computational cost. Our goal is to benefit from the EVSS formulation without increase in the problem size. We have reformulated the convective term by explicitly considering the divergence-free nature of the velocity field. The proposed identity based on the tensor calculus helped to retain the problem size to three field formulation with the ability to move the higher order derivatives to the test function in the weak formulation.

2 Mathematical equations

In this paper, we shall consider the incompressible, stationary EVSS formulation obtained by the introduction of splitting (1) to the standard viscoelastic formulation [11]. The equation of motion for Stokes flow is characterized by extremely low Reynolds numbers such that the viscous forces outweigh inertial forces. The EVSS formulation is mathematically expressed as,

$$-2\eta_0 \nabla \cdot \mathbf{D}(\mathbf{u}) + \nabla p - \nabla \cdot \boldsymbol{E} = 0 \tag{2a}$$

$$\nabla \cdot \mathbf{u} = 0 \tag{2b}$$

$$\lambda(2\eta_p \overset{\nabla}{\mathbf{D}}(\mathbf{u}) + \overset{\nabla}{\boldsymbol{E}}) + f\left(2\eta_p \mathbf{D}(\mathbf{u}) + \mathbf{E}, \lambda\right)\left(2\eta_p \mathbf{D}(\mathbf{u}) + \mathbf{E}\right) + h\left(2\eta_p \mathbf{D}(\mathbf{u}) + \mathbf{E}\right) = 2\eta_p \mathbf{D}(\mathbf{u}) \tag{2c}$$

Equations (2a) and (2b) are the Stokes equations coupled with an additional stress equation (2c). In the above mentioned formulation, $\mathbf{u}, p$ and $\boldsymbol{E}$ are the field variables that indicate the fluid's velocity, pressure and elastic part of the extra stress tensor, respectively. The deformation tensor $\mathbf{D}(\mathbf{u})$ is the symmetric part of the velocity gradient. The parameters λ and η_0 are the relaxation time and the total viscosity, respectively. The relaxation time λ characterizes the elastic properties of the fluid. For simplicity, we set the total viscosity

$\eta_0 = \eta_s + \eta_p = 1$ which is the composition of the solvent viscosity and the polymer viscosity. Having zero contribution from the solvent viscosity, i.e. η_s=0, results in the pure polymer viscoelastic formulation. The terms $\overset{\nabla}{\boldsymbol{E}}$ and $\mathbf{D}\overset{\nabla}{(\mathbf{u})}$ represent the upper-convected derivative of the elastic part of the extra-stress tensor and the deformation tensor, respectively.

$$\overset{\nabla}{\boldsymbol{E}} = (\mathbf{u}\cdot\nabla)\,\boldsymbol{E} - \nabla\mathbf{u}^T\cdot\boldsymbol{E} - \boldsymbol{E}\cdot\nabla\mathbf{u} \tag{3}$$

$$\overset{\nabla}{\mathbf{D}}(\mathbf{u}) = (\mathbf{u}\cdot\nabla)\,\mathbf{D}(\mathbf{u}) - \nabla\mathbf{u}^T\cdot\mathbf{D}(\mathbf{u}) - \mathbf{D}(\mathbf{u})\cdot\nabla\mathbf{u} \tag{4}$$

The specific viscoelastic model is defined by the functions $f\,(2\eta_p\mathbf{D}(\mathbf{u}) + \mathbf{E}, \lambda)$ and $h(2\eta_p\mathbf{D}(\mathbf{u}) + \mathbf{E})$ in equation (2c). The constitutive equation for the simplest Oldroyd-B model [12] is obtained by setting $f\,(2\eta_p\mathbf{D}(\mathbf{u}) + \mathbf{E}, \lambda)$=1 and $h\,(2\eta_p\mathbf{D}(\mathbf{u}) - \mathbf{E})$=0,

$$\lambda\overset{\nabla}{\boldsymbol{E}} + \boldsymbol{E} = -2\eta_p\lambda\overset{\nabla}{\mathbf{D}}(\mathbf{u})\,. \tag{5}$$

Giesekus model [13] is derived by defining $f\,(2\eta_p\mathbf{D}(\mathbf{u}) + \boldsymbol{\zeta}, \lambda)$=1 and $h\,(2\eta_p\mathbf{D}(\mathbf{u}) + \boldsymbol{\zeta}) \neq 0$

$$\lambda\overset{\nabla}{\boldsymbol{E}} + \boldsymbol{E} + \frac{\alpha\lambda}{\eta_p}\left((2\eta_p\mathbf{D}(\mathbf{u}) + \mathbf{E})\cdot(2\eta_p\mathbf{D}(\mathbf{u}) + \mathbf{E})\right) = -2\eta_p\lambda\overset{\nabla}{\mathbf{D}}(\mathbf{u}) \tag{6}$$

where $\alpha \in [0, 1]$ refers to the mobility factor. The PTT (Phan-Thien-Tanner) exponential model [14] is obtained for $f\,(2\eta_p\mathbf{D}(\mathbf{u}) + \mathbf{E}, \lambda)$= function and $h\,(2\eta_p\mathbf{D}(\mathbf{u}) + \mathbf{E})$=0

$$\lambda(2\eta_p\overset{\nabla}{\mathbf{D}}(\mathbf{u}) + \overset{\nabla}{\boldsymbol{E}}) + \exp\left(\frac{\lambda\kappa}{\eta_p}\left(\mathrm{Tr}\ (2\eta_p\mathbf{D}(\mathbf{u}) + \mathbf{E})\right)\right)(2\eta_p\mathbf{D}(\mathbf{u}) + \mathbf{E}) = 2\eta_p\mathbf{D}(\mathbf{u}) \tag{7}$$

where $\kappa \in [0, 1]$ is the extensibility parameter. The constitutive equation of the Giesekus and PTT exponential model simplifies to the Oldroyd-B model at α=0 and κ=0, respectively. In order to obtain a well-posed mathematical problem the set of governing equations is subject to suitable boundary conditions. The Dirichlet data is prescribed regarding the velocity field on all the boundaries. The inflow stress is set in accordance to the inflow velocity. On the remaining boundary edges, a so-called do-nothing boundary condition [15] is imposed.

3 Numerical Challenges

Handling viscoelastic models computationally presents significant challenges, especially when dealing with pure polymer viscoelastic formulations. This results in the absence of the diffusion operator in the momentum equation, making both discretization and solution techniques difficult. Employing the EVSS formulation allows us to effectively reintroduce the diffusive operator, thereby reintroducing the velocity coupling into the momentum equation. While the velocity coupling is recovered in the momentum equation, additional terms appear in the constitutive equation for stress. The convected derivative of the rate of deformation tensor involves second-order velocity derivatives, which pose significant computational challenges. To address these complexities, a common approach is to expand the problem size to a four-field formulation by introducing deformation tensor as an additional variable which increases the computational cost. Keeping in view the divergence free nature of the velocity field the convective term is reformulated to deal with the higher order derivates. An identity for the second-order tensor field $\boldsymbol{L}$ and a solenoidal vector field $\mathbf{v}$ can be derived by employing the tensor calculus and Einstein's summation convention [16].

$$\nabla\cdot(\boldsymbol{L}\otimes\mathbf{v}) = \mathbf{v}\cdot\nabla\boldsymbol{L} + (\nabla\cdot\mathbf{v})\,\boldsymbol{L} \tag{8}$$

In equation (8), the dyadic product of two vectors is represented by $\otimes$. By setting $\boldsymbol{L} = \mathbf{D}(\mathbf{u})$ and $\mathbf{v} = \mathbf{u}$ in equation (4) leads to,

$$\overset{\nabla}{\mathbf{D}} = \nabla \cdot (\mathbf{u} \otimes \mathbf{D}(\mathbf{u})) - \nabla \mathbf{u}^T \cdot \mathbf{D}(\mathbf{u}) - \mathbf{D}(\mathbf{u}) \cdot \nabla \mathbf{u} \tag{9}$$

This formulation offers the possibility to shift the higher order derivatives onto the test function in the weak formulation via partial integration. Thus, pertaining the problem size to three field formulation.

4 Solution strategies

The EVSS formulation aids in recovering the diffusive operator in the momentum equation, thereby enabling the problem to be treated in a decoupled fashion. Furthermore, another advantage of the EVSS formulation lies in its potential to be solved in a fully monolithic way. Numerical computations are performed employing both the decoupled and monolithic approaches for the three-field viscoelastic fluids.

4.1 Decoupled approach

In the decoupled approach, the three field formulation is split into two subproblems i.e. the Stokes part and the constitutive equation for stress. The velocity obtained from the Stokes part is employed in the constitutive equation and the corresponding stress obtained from the constitutive equation is updated in the momentum equation of the Stokes part in each iteration. Let $(\mathbf{u}^n, p^n, \boldsymbol{E}^n)$ be the known approximation of $(\mathbf{u}, p, \boldsymbol{E})$ after n steps. The step $(n+1)$ of the algorithm consists of first computing $(\mathbf{u}^{n+1}, p^{n+1})$ by solving the Stokes equation using the previous stress $\boldsymbol{E}^n$ in the right-hand side of the linear system, and then computing $\boldsymbol{E}^{n+1}$ by using its constitutive equation. The iteration $(n+1)$ consists of first computing $(\mathbf{u}^{n+1}, p^{n+1})$ as follows:

$$\begin{aligned} -2\eta_0 \nabla \cdot \mathbf{D}\left(\mathbf{u}^{n+1}\right) + \nabla p^{n+1} &= \nabla \cdot \boldsymbol{E}^n \\ \nabla \cdot \mathbf{u}^{n+1} &= 0 \end{aligned} \tag{10}$$

and in the second step compute $\boldsymbol{E}^{n+1}$,

$$\begin{aligned} \lambda\Big(2\eta_p \left(\nabla \cdot \left(\mathbf{u}^{n+1} \otimes \mathbf{D}\left(\mathbf{u}^{n+1}\right)\right) - \nabla \mathbf{u}^{Tn+1} \cdot \mathbf{D}\left(\mathbf{u}^{n+1}\right) - \mathbf{D}\left(\mathbf{u}^{n+1}\right) \cdot \nabla \mathbf{u}^{n+1}\right) + \\ \left(\mathbf{u}^{n+1} \cdot \nabla\right) \boldsymbol{E}^{n+1} - \nabla \mathbf{u}^{Tn+1} \cdot \boldsymbol{E}^{n+1} - \boldsymbol{E}^{n+1} \cdot \nabla \mathbf{u}^{n+1}\Big) + h\left(2\eta_p \mathbf{D}\left(\mathbf{u}^{n+1}\right) + \boldsymbol{E}^{n+1}\right) + \\ f\left(2\eta_p \mathbf{D}\left(\mathbf{u}^{n+1}\right) + \boldsymbol{E}^n, \lambda\right)\left(2\eta_p \mathbf{D}\left(\mathbf{u}^{n+1}\right) + \boldsymbol{E}^{n+1}\right) - 2\eta_p \mathbf{D}\left(\mathbf{u}^{n+1}\right) = 0 \end{aligned}$$

4.2 Monolithic approach

The set of equations described in (2) can be solved in a monolithic manner that means to solve the velocity-pressure-stress equation simultaneously. The set of non-linear equations is linearized using the outer fixed-point solver. Let $(\mathbf{u}^n, p^n, \boldsymbol{E}^n)$ be the known approximation

of $(\mathbf{u}, p, \boldsymbol{E})$ after n steps. The iteration $(n+1)$ consists of:

$$
\begin{aligned}
-2\eta_0 \nabla \cdot \mathbf{D}\left(\mathbf{u}^{n+1}\right) + \nabla p^{n+1} - \nabla \cdot \boldsymbol{E}^{n+1} &= 0 \\
\nabla \cdot \mathbf{u}^{n+1} &= 0 \\
\lambda\Big(2\eta_p \left(\nabla \cdot \left(\mathbf{u}^n \otimes \mathbf{D}\left(\mathbf{u}^{n+1}\right)\right) - \nabla \mathbf{u}^{Tn} \cdot \mathbf{D}\left(\mathbf{u}^{n+1}\right) - \mathbf{D}\left(\mathbf{u}^{n+1}\right) \cdot \nabla \mathbf{u}^n\right) + \\
\left(\mathbf{u}^n \cdot \nabla\right) \boldsymbol{E}^{n+1} - \nabla \mathbf{u}^{Tn} \cdot \boldsymbol{E}^{n+1} - \boldsymbol{E}^{n+1} \cdot \nabla \mathbf{u}^n\Big) + h\left(2\eta_p \mathbf{D}\left(\mathbf{u}^{n+1}\right) + \boldsymbol{E}^{n+1}\right) + \\
f\left(2\eta_p \mathbf{D}\left(\mathbf{u}^n\right) + \boldsymbol{E}^n, \lambda\right)\left(2\eta_p \mathbf{D}\left(\mathbf{u}^{n+1}\right) + \boldsymbol{E}^{n+1}\right) - 2\eta_p \mathbf{D}\left(\mathbf{u}^{n+1}\right) &= 0
\end{aligned}
$$

The set of equations in the matrix-vector notation are written as

$$
\begin{bmatrix} A & B & R \\ B^T & 0 & 0 \\ K(\mathbf{u}^n) & 0 & Z(\mathbf{u}^n) \end{bmatrix} \begin{bmatrix} \mathbf{u} \\ p \\ \boldsymbol{E} \end{bmatrix} = \begin{bmatrix} \boldsymbol{r}_{\mathbf{u}} \\ \boldsymbol{r}_p \\ \boldsymbol{r}_{\boldsymbol{E}} \end{bmatrix}
$$

5 Finite Element discretization

The finite element method is chosen for the discretization in space. The set of equations given above describes the strong form of the three field formulation. In order to work with the numerical flow simulations using finite element method, we convert the equations from the strong form to the weak form which allows one to lower the continuity restrictions on the approximating subspaces. The weak formulation is obtained by multiplying the test functions $\boldsymbol{v}, q$ and $\boldsymbol{\phi}$ for the velocity, pressure and stress, respectively, to the system of equations in (2) and by integrating over the domain. The equations in the weak formulation after applying integration by parts read as,

$$
\begin{aligned}
2\eta_0 \int_\Omega \mathbf{D}(\mathbf{u}) : \mathbf{D}(\boldsymbol{v})\, dx - \int_\Omega p \nabla \cdot \boldsymbol{v}\, dx + \int_\Omega \boldsymbol{E} : \mathbf{D}\left(\boldsymbol{v}\right)\, dx &= 0 \\
\int_\Omega q\, \nabla \cdot \boldsymbol{u}\, dx &= 0 \\
\int_\Omega f\left(2\eta_p \mathbf{D}\left(\mathbf{u}\right) + \mathbf{E}\lambda\right)\left(2\eta_p \mathbf{D}\left(\mathbf{u}\right) + \mathbf{E}\right) : \boldsymbol{\phi}\, dx + & \\
\int_\Omega \lambda(2\eta_p \overset{\nabla}{\mathbf{D}}(\mathbf{u}) + \overset{\nabla}{\boldsymbol{E}}) : \boldsymbol{\phi}\, dx + \int_\Omega h\left(2\eta_p \mathbf{D}\left(\mathbf{u}\right) + \mathbf{E}\right) : \boldsymbol{\phi}\, dx &= \int_\Omega 2\eta_p \mathbf{D}\left(\boldsymbol{u}\right) : \boldsymbol{\phi}\, dx
\end{aligned}
$$

where,

$$
\int_\Omega \overset{\nabla}{\mathbf{D}}(\mathbf{u}) : \boldsymbol{\phi}\, dx = -\int_\Omega \left(\mathbf{u} \otimes \mathbf{D}\left(\mathbf{u}\right)\right) : \nabla \boldsymbol{\phi}\, dx - \int_\Omega \left(\nabla \mathbf{u}^T \cdot \mathbf{D}\left(\mathbf{u}\right) + \mathbf{D}\left(\mathbf{u}\right) \cdot \nabla \mathbf{u}\right) : \boldsymbol{\phi}\, dx \tag{11}
$$

The unknown field variables for the velocity, pressure and stress are approximated in vector-scalar-tensor valued function spaces $\mathbb{V} \times \mathbb{Q} \times \mathbb{X}$, respectively. Let us define the conforming finite element spaces $V_h \subset V$, $X_h \subset X$ and the piecewise discontinuous finite element space $Q_h \subset Q$ such that,

$$
\begin{aligned}
\mathbb{V}_h &= \{\boldsymbol{v}_h \in \mathbb{V},\ \boldsymbol{v}_{h|T} \in (Q_2(K))^2\ \forall\ K \in T_h\} \\
\mathbb{Q}_h &= \{q_h \in \mathbb{Q},\ q_{h|T} \in (P_1^{disc}(K))\ \forall\ K \in T_h\} \\
\mathbb{X}_h &= \{\boldsymbol{\phi}_h \in \mathbb{X},\ \boldsymbol{\phi}_{h|T} \in (Q_3(K))^{2\text{x}2}\ \forall\ K \in T_h\}
\end{aligned} \tag{12}
$$

The choice of the FEM spaces for the Stokes problem is subject to the well-known compatibility condition between the velocity and pressure spaces, the so-called inf-sup condition given in discrete version (LBB)[17].

$$sup_{\mathbf{u}\in\mathbb{V}_h}\frac{\int_\Omega \nabla\cdot\mathbf{u}\; q dx}{||\mathbf{u}||_{1,\Omega}} \geq \zeta||q||_{0,\Omega} \qquad\qquad \forall q\in\mathbb{Q}_h \tag{13}$$

There are a vast number of finite element spaces satisfying the inf-sup condition for the velocity pressure coupling. Similarly, adding the weak form of the constitutive equation for $\boldsymbol{E}$ imposes further compatibility constraints onto the choice of the approximations spaces for the triple velocity-pressure-stress

$$sup_{\boldsymbol{E}\in\mathbb{X}_h}\frac{\int_\Omega \nabla\cdot\boldsymbol{E}\;\mathbf{u} dx}{||\boldsymbol{E}||_{0,\Omega}} \geq \xi||\mathbf{u}||_{1,\Omega} \qquad\qquad \forall\mathbf{u}\in\mathbb{V}_h \tag{14}$$

where ζ and ξ are two mesh-independent constants and $||.||_{1,\Omega}$ and $||.||_{0,\Omega}$ are the standard $H^1(\Omega)$ and $L^2(\Omega)$ norms, respectively. From the numerical point of view, conditions (13) and (14) must be satisfied in the finite element subspaces to lead to a stable scheme. Element pairs that satisfy equation are also said to be compatible. Fortin and Pierre [18] have shown that in the absence of the viscous contribution, the standard discrete spaces have to satisfy the following conditions:

1. The velocity-pressure spaces must be compatible with respect to equation
2. If the elastic stress tensor $\boldsymbol{E}$ is approximated by a discontinuous FEM space, the deformation tensor must be a member of the same space

$$\mathbf{D}(\mathbf{u}) = \frac{1}{2}(\nabla\mathbf{u}+\nabla\mathbf{u}^T) \;\in\; \mathbb{X}_h \qquad \forall\,\mathbf{u}\in\;\mathbb{V}_h \tag{15}$$

3. If the stress tensor is approximated by a continuous FEM space, the number of local degrees of freedom must be larger than that used for the velocity space.

In this paper, the flow domain Ω is discretized by means of quadrilaterals. The velocity $\mathbf{u}$ is approximated by continuous biquadratic (9 nodes) polynomials while the pressure p is approximated by piecewise discontinuous linear polynomials. This well-known choice Q_2/P_1^{disc} satisfies the LBB condition for the velocity-pressure formulation. It is known to be one of the *most popular* Stokes elements since it is a quite accurate and robust finite element pair for highly viscous incompressible flow. When dealing with the viscoelastic formulation, the real challenge lies in fulfilling condition (14) while meeting one of the last two requirements. The discontinuous Galerkin technique used by Fortin and Fortin [19] can satisfy the LBB requirement if the stress tensor is approximated in the discontinuous space. Marchal and Crochet [20] have proposed a subcell discretization to enrich the local degrees of freedom for the stress space, thus fulfilling the third requirement. We have approximated the stress tensor $\boldsymbol{E}$ by continuous bicubic (16 nodes) polynomials i.e. Q_3 finite element. Thus, the stable finite element triplet for the three field viscoelastic formulation velocity, pressure and stress field is $Q_2/P_1^{disc}/Q_3$ shown in Figure 1.

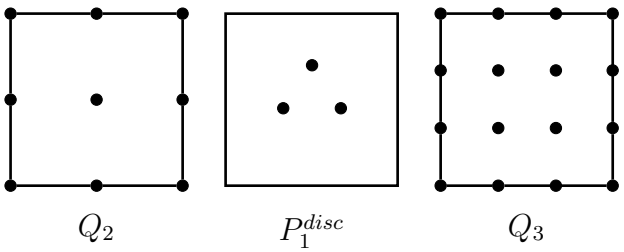

Figure 1: Finite elements Q_2,P_1^{disc},Q_3 for velocity, pressure and stess, respectively.

Convection-dominated flows can be stabilized by adding an edge-oriented stabilization (EOFEM) term [21] into the discrete system diagonal blocks, penalizing the jump of the solution gradient across element edges given as,

$$j_{\mathbf{u}} = \sum_{E} \gamma_{\mathbf{u}} \left(h_E\right)^p \int_E [\mathbf{D}\left(\mathbf{u}\right)] : [\mathbf{D}\left(\boldsymbol{v}\right)] ds \tag{16}$$

where $\gamma_{\mathbf{u}}$ is the mesh independent scaling factor for the jump stabilization operator, h_E is the length of the edge and the exponent p is the power of appropriate order [21].

6 Numerical results

The numerical computations are performed on the computer servers of TU Dortmund University using the FEAT3 software, which is a novel C++ code with a highly adaptable solver structure that is intended for usage by researchers as well as in industry applications. The link to the code can be found on the GitHub page [1]. Numerical simulations are performed using both the decoupled and monolithic approaches for the Oldroyd-B, Giesekus, and PTT exponential model, utilizing the outer non-linear fixed point solver and the inner linear direct solver UMFPACK. The convergence is ensured when the norm of the defect vectors meets a specified tolerance. The numerical results are obtained on the four-to-one contraction [22] because of its great importance in several processing operations, such as molding and extrusion of viscoelastic materials. However, in industrial processes, especially for 4:1 contraction problems, there are many obstacles when fluid passes through a part of an abrupt contraction. Thus, the geometrical domain of this problem for sharp corners is changed to rounded corners. The rounded geometry is generated by Brown et. al. [23] with a curve segment at contraction to reduce the severe stress. Moreover, taking advantage of the symmetry in the four-to-one contraction, only half of the domain is utilized for the computations. This reduces the number of elements for the numerical computations by half, i.e. 3968 quadrilaterals at mesh refinement level 3 thus providing somewhat numerical ease. The underlying geometry in Figure 2 is a 4:1 curved contraction ($y_{in} \in (0, +4)\,, y_{out} \in (0, +1)$). The boundary functions are specific to each viscoelastic model.

Figure 2: Configuration for 4:1 contraction flow

[1] https://github.com/tudo-math-ls3/feat3

6.1 Oldroyd-B model

Among the viscoelastic models, Oldroyd-B model is the simplest and therefore often selected as the first model for computations because of the availability of the analytic functions for the velocity and stress. The following parabolic velocity and the stress functions are prescribed at the inflow of the contraction

$$\mathbf{u} = \begin{pmatrix} U\,(16 - y^2/16) \\ 0 \end{pmatrix}, \quad \boldsymbol{E} = \begin{pmatrix} \frac{1}{32}\lambda\eta_p U^2 y^2 & 0 \\ 0 & 0 \end{pmatrix} \tag{17}$$

where η_p=1 and U=0.4. The numerical results are computed for different values of the material parameter λ. The Newtonian flow is recovered at λ=0 while the viscoelastic results are obtained for $\lambda > 0$. The limits of the relaxation parameter λ are recorded in the current setting by employing the decoupled and monolithic solution approaches. As the viscoelastic effects are intensified by increasing the relaxation parameter λ, the difficulty level to solve the problem increases. Out of both solution approaches, the decoupled formulation is less expensive in terms of the time and memory as seen in Table 1. The computations are performed on compute server with Intel Xeon E5-2640 v3 with 16 cores and 218 GiB DDR4 Memory.

λ	**Decoupled**			**Monolithic**		
	Iterations	**Run Time (sec)**	**Memory (GB)**	**Iterations**	**Run Time (sec)**	**Memory (GB)**
0.0	2	08	0.951	2	13	1.551
0.5	29	167	1.119	5	81	1.787
1.0	59	334	1.121	15	243	1.834
3.0	181	1048	1.131	86	2048	2.100
5.0	1091	6222	1.129	-	-	-

Table 1: Computation cost for the Oldroyd-B viscoelastic model

The monolithic approach is more robust as it has the ability to solve for all the field variables simultaneously. At λ=5 no convergence could be obtained for the monolithic formulation. However, the robustness of the monolithic formulation is supported by the convergence plots in Figure 3 where it can be observed that the EOFEM parameter $\gamma_{\mathbf{u}}$ has little to no influence on the velocity and stress convergence plots obtained by the monolithic formulation while the decoupled approach is heavily influenced by the addition of the stabilization.

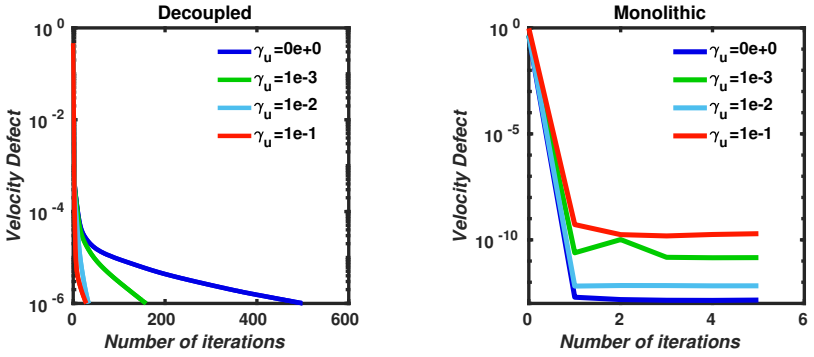

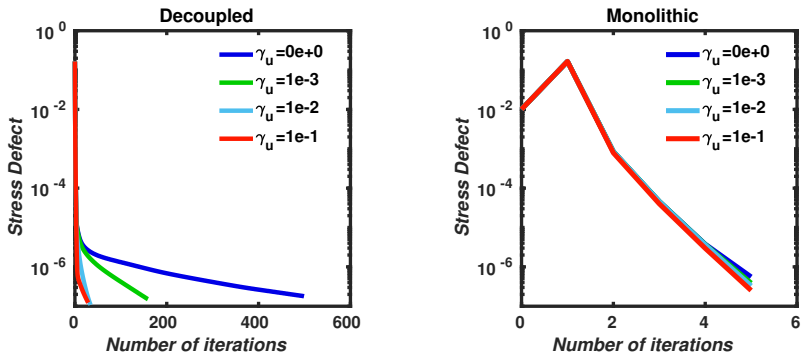

Figure 3: Effects of the EOFEM on the Oldroyd-B Model at $\lambda = 0.5$

As already mentioned, Oldroyd-B is the simplest viscoelastic model such that it is unable to capture any realistic or meaningful viscoelastic material behaviour. For example, this can be realised based on the corresponding fully developed parabolic velocity profile from the velocity function in equation (17), which is independent of the relaxation time λ. Consequently, no modelling of any nonlinear effects such as shear thinning, which occurs for increasing relaxation times, is possible. Thus, results for the Giesekus and PTT exponential model are computed that indeed depict the viscoelastic effects such that the flow profiles deviate from the parabolic shape.

6.2 Giesekus Model

The Giesekus model is obtained by the introduction of an additional quadratic stress contribution to the Oldroyd-B model. The model is capable of predicting a shear thinning effect by specifying the nonlinear material parameter $\alpha \in [0, 1]$. When considering parabolic profiles as the inflow function to compute fully developed viscoelastic flow profiles in simulating viscoelastic Poiseuille flow using the Giesekus model, inappropriate flow phenomena is observed. It is evident that the chosen parabolic velocity profile is not suitable, as the velocity field exhibits a different shape away from the inflow and outflow edges. This contradicts the expected numerical results for Poiseuille flow as shown by the study of Westervoß [16]. Therefore, the fully developed flow profiles resulting in case of the Giesekus model are evaluated with respect to the included material and model parameter and pressure drop with the help of the following semi-analytic expression of the velocity profile in the non-solvent case given in [24].

$$u_1(y) = \frac{B}{\lambda}\Big[\left(1-2\beta^2\right) log\frac{\beta+\sqrt{1-\phi^2\frac{y^2}{B^2}}}{\beta+\sqrt{1-\phi^2}} + \beta\left(\sqrt{1-\phi^2\frac{y^2}{B^2}} - \sqrt{1-\phi^2}\right) + \beta\left(1-\beta^2\right)\left(\frac{1}{\beta+\sqrt{1-\phi^2\frac{y^2}{B^2}}} - \frac{1}{\left(\beta+\sqrt{1-\phi^2}\right)}\right)\Big]/\phi \tag{18}$$

u_2=0. In the above expression $\beta = 2\alpha - 1$ and $\phi = 2\alpha\lambda P_x$, where α=0.1. The corresponding stress function is given as,

$$\boldsymbol{E} = \begin{pmatrix} \frac{(1-\alpha)\left(1 \mp \sqrt{1-4\alpha^2 \frac{\lambda^2 P_x^2 y^2}{B^2}} + 2\alpha^2 \frac{\lambda P_x y}{B}\right)}{\alpha\left(2\alpha - 1 \pm \sqrt{1-4\alpha^2 \frac{\lambda^2 P_x^2 y^2}{B^2}}\right)} & \frac{\lambda P_x y}{B} \\ \frac{\lambda P_x y}{B} & \frac{-1 \pm \sqrt{1-4\alpha^2 \frac{\lambda^2 P_x^2 y^2}{B^2}}}{2\alpha} \end{pmatrix} \tag{19}$$

The velocity function is characterized by a y-dependent term in the x-direction, while the extra-stress tensor components vary solely with respect to the channel height. The application of these properties to the steady-state Giesekus model yields a nonlinear system of ordinary differential equations (ODEs) in one dimension. The pressure drop P_x in the above function is obtained by solving the one-dimensional nonlinear set of equations such that the velocity profile results in the desired flow rate. Subsequently, this determined pressure drop value is incorporated into the velocity and stress functions to prescribe the relevant boundary conditions in our 2-D code. The study of Ferras et al. [24] shows that the lower branch solution exhibits physically unrealistic solutions and therefore only the upper branch solution can be considered for the numerical simulations. Similar to Oldroyd-B, the monolithic formulation for the Giesekus model appears to be more robust by not being influenced by the stabilization parameter as shown in Figure 4. The increase in the stabilization parameter $\gamma_{\mathbf{u}}$ in the decoupled formulation helps to attain the velocity and stress convergence in less iterations thus facilitating the convergence while the monolithic convergence is independent of the parameter $\gamma_{\mathbf{u}}$ for smaller values of the relaxation parameter.

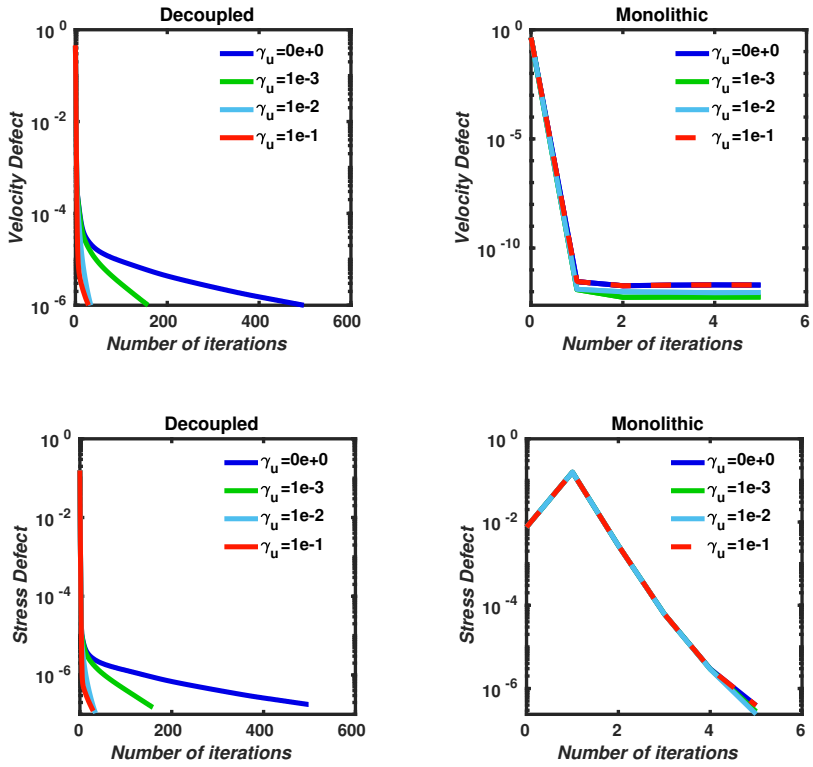

Figure 4: Effects of the EOFEM on the Giesekus Model at $\lambda = 0.5$

The decoupled formulation takes the lead from the monolithic approach in terms of computational cost as shown in Table 2. The 'price' to be paid for the enhanced robustness properties

of such monolithic approach is the more expensive solution of the resulting coupled discrete nonlinear system. While decoupled/operator-splitting schemes, reduce the complete solution to a sequence of much simpler sub problems, the outer coupling of such subproblems is still a challenging problem, in the case of high relaxation parameters for the Giesekus and PTT exponential model.

λ	**Decoupled**			**Monolithic**		
	Iterations	**Run Time (sec)**	**Memory (GB)**	**Iterations**	**Run Time (sec)**	**Memory (GB)**
0.1	6	40	1.093	4	45	1.699
0.5	29	170	1.117	5	82	1.783
1.0	59	340	1.121	7	122	1.835
3.0	168	974	1.127	53	1279	2.109
5.0	345	1986	1.127	186	4804	2.160

Table 2: Computational cost for the Giesekus viscoelastic model

The similar numerical solution technique needs to be applied in case of the PTT exponential model. The PTT exponential model provides the analogous numerical solutions to the Giesekus model. However, for completeness, the PTT exponential model is briefly analysed in the next section.

6.3 PTT exponential Model

The flow profiles for the PTT exponential model are evaluated with respect to the effect of the included material parameter on the nonlinearity of the solution. Similar to the Giesekus model, the PTT exponential model is capable of predicting a shear thinning effect by specifying the nonlinear material parameter κ=0.1. The following semi-analytic expression of the velocity profile in the non-solvent case is prescribed by [24] for the PTT exponential model,

$$u_1(y) = \frac{\eta_p}{4\kappa\lambda^2\frac{\partial p}{\partial x}}\left[exp\left(2\kappa\left(\frac{\lambda}{\eta_p}\frac{\partial p}{\partial x}\left(y-\frac{b+a}{2}\right)\right)^2\right) - exp\left(2\kappa\left(\frac{\lambda}{\eta_p}\frac{\partial p}{\partial x}\left(\frac{b-a}{2}\right)\right)^2\right)\right] \tag{20}$$

u_2=0. The corresponding stress profile is,

$$\boldsymbol{E} = \begin{pmatrix} \frac{2\lambda}{\eta_p}\left(\frac{\partial p}{\partial x}y\right)^2 & \frac{\partial p}{\partial x}y\left(1-exp\left(2\kappa\left(\frac{\lambda}{\eta_p}\frac{\partial p}{\partial x}y\right)^2\right)\right) \\ \frac{\partial p}{\partial x}y\left(1-exp\left(2\kappa\left(\frac{\lambda}{\eta_p}\frac{\partial p}{\partial x}y\right)^2\right)\right) & 0 \end{pmatrix}$$

The pressure drop $\frac{\partial p}{\partial x}$ for the PTT exponential model is determined in a similar manner to the Giesekus model. Identical convergence behavior is observed for the PTT exponential model and is therefore not included. The computational cost for the PTT exponential model is given in Table 3.

λ	Decoupled			Monolithic		
	Iterations	**Run Time (sec)**	**Memory (GB)**	**Iterations**	**Run Time (sec)**	**Memory (GB)**
0.1	6	40	1.096	3	64	1.749
0.5	29	182	1.114	7	103	1.714
1.0	59	369	1.114	15	321	2.034
3.0	150	927	1.128	66	1539	2.095
10.0	962	5849	1.132	-	-	-

Table 3: Computational cost for the PTT exponential viscoelastic model

The decoupled PTT exponential routine predicts the viscoelastic effects in a quite realistic manner by being able to achieve results at a very high relaxation time $\lambda = 10$ where no convergence could be achieved for the monolithic approach. It would be quite fascinating and interesting to visualize the flow behavior specially near the contraction in Figure 5 at high relaxation parameter λ.

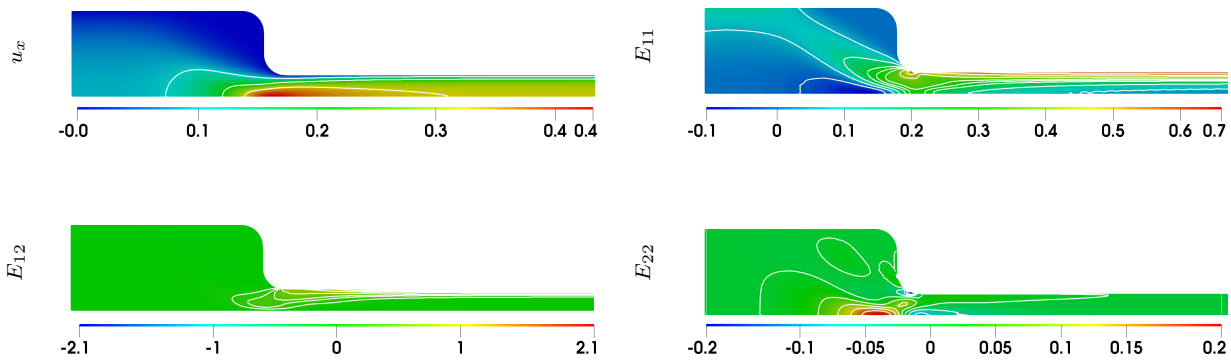

Figure 5: Components of tensor $\boldsymbol{E} \in Q3$ for PTT exponential model at relaxation parameter $\lambda = 50$ at mesh refinement level 3

The horizontal velocity u_x in Figure 5 deviates from the parabolic line shape due to the shear thinning effect, which shows the maximum value at the symmetry line only at the beginning of the downstream channel and later produces a plateau-like behavior. The contours of the stress components E_{11} and E_{12} show the maximum value near the location of the curved corner contraction where there is a the sudden change in geometry from 4 unit reduced to 1 unit as well as along the channel wall. This behavior is in accordance with the stress function given above. The stress component E_{22} shows the line contour with the maximum value being near the location of the curved corner contraction and the symmetry line where the fluid pass through the sudden change in geometry. Being able to obtain the results at a very high relaxation parameter λ convinced us to continue to work in future with the PTT exponential model in a decoupled routine. We aim to establish an algorithm with such solver settings that enable realistic predictions of the viscoelastic behavior efficiently without encountering any limitation in the relaxation parameter λ.

6.4 Shear thinning effect

Viscoelastic materials show a so-called shear thinning behaviour, that is a decreasing shear viscosity which is observed for increasing shear rates. The flow profiles calculated for the Giesekus and the PTT exponential model in terms of fully developed channel flow configurations show a reasonable behaviour under variation of the relaxation time λ. For increasing relaxation times, a typical shear thinning behaviour can be observed regarding the velocity profiles depicted in Figure 6, which is one of the main material properties predicted by the Giesekus and PTT exponential model. In case of shear thinning, the velocity profile deviates from the parabolic profile, such that a large velocity gradient arises close to the walls, while a plateau-like behaviour begins to appear at the downstream of the channel. This plateau effect becomes more prominent as the relaxation parameter is further increased. Furthermore, a very good agreement to the semi-analytical reference solution given in [24] is observed on a visual basis.

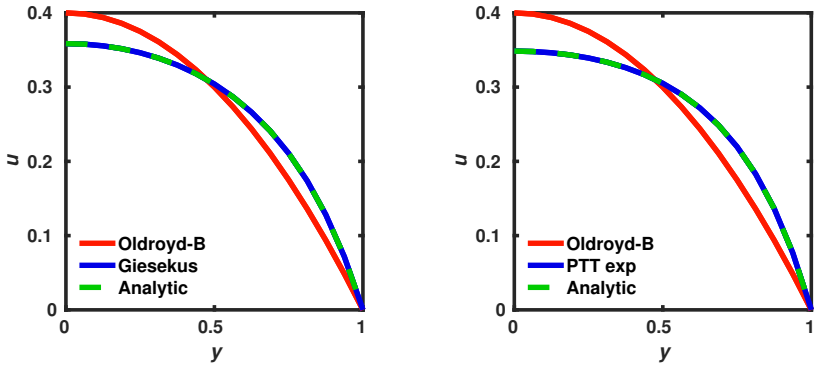

Figure 6: Shear thinning effect produced by Giesekus and PTT exponential model at λ= 5 and 10, respectively at the downstream channel x=20.

7 Summary

In this paper, the EVSS approach to simulate viscoelastic fluid flows is utilized with special emphasis on pure polymer melts, that is viscoelastic fluids without a solvent contribution to the viscosity. On one hand, utilizing the EVSS formulation, the velocity coupling is recovered in the momentum equation making it feasible to be solved by a decoupled as well as a monolithic approach. On the other hand, second order velocity derivatives appear in the convective term of the constitutive equation for stress which is quite difficult to handle computationally. In this research work, the convective term is reformulated by explicitly considering the divergence-free nature of the velocity field. The proposed identity based on the tensor calculus helped to retain the problem size to three field formulation with the ability to move the higher order derivatives to the test function in the weak formulation. Furthermore, the discrete spaces regarding the velocity and stress fields need to satisfy an additional inf-sup or LBB condition in order to obtain a stable mixed Finite Element formulation of the viscoelastic model. Therefore, the $Q_2/P_1^{disc}/Q_3$ finite element triplet is selected for the velocity, pressure and the stress space. Certain limits of the relaxation parameter λ are observed by employing both the decoupled and monolithic approach for all three viscoelastic models. As the relaxation parameter λ is increased, the viscoelastic effects increase that means fluid begins to behave more like solid as compared to liquid which in turn arises the numerical difficulties. It is worth noting in the monolithic formulation, the limitation to achieve the results at higher λ could possibly be due to fixed point solver

instead of the Newton solver which necessitates the calculation of the Jacobian and poses challenges in the implementation. For the decoupled approach, an alternative solver or a non-stationary environment may be considered. Out of the three viscoelastic models, the PTT exponential model seems to produce the realistic flow behavior especially for the decoupled approach where the results at comparatively high values of the relaxation parameter are achieved. We are committed to exploring strategies to overcome the limitations and advance the capabilities of both solution approaches for the PTT exponential model in future.

Acknowledgments

We would like to thank the Deutscher Akademischer Austauschdienst (DAAD) for their financial support. The authors also acknowledge the support by LS3 and LiDO3 team at ITMC, TU Dortmund University.

REFERENCES

[1] M.Perera and K. Walters, Long- range memory effects in flows involving abrupt changes in geometry, Part I. Flows associated with L-shaped and T-shaped geometries, *J. Non-Newtonian Fluid Mech*, **2**, 49–81, (1977).

[2] M.A. Mendelson, P.W. Yeh, R.C. Armstrong, R.A. Brown, Approximation error in finite element calculation of viscoelastic fluid flows, *J. Non-Newtonian Fluid Mech.*, **10**, 31-54, (1982).

[3] A.N. Beris, R.C. Armstrong, R.A. Brown, Finite element calculation of viscoelastic flow in a Journal bearing. I. Small eccentricities, *J. Non-Newtonian Fluid Mech.*, **16**, 141-172, (1984).

[4] A.N. Beris, R.C. Armstrong, R.A. Brown, finite element calculation of viscoelastic flow in a Journal bearing. II. Moderate eccentricities, *J. Non-Newtonian Fluid Mech.*, **19**, 323-347, (1986).

[5] D. Rajagopalan, R. C. Armstrong and R. A. Brown, Finite element methods for calculation of steady, viscoelastic flow using constitutive equations with a Newtonian viscosity, *J. Non-Newtonian Fluid Mech.*, **36**, (1990).

[6] F.P.T. Baaijens, Mixed finite element methods for viscoelastic flow analysis: A review, *J. Non-Newtonian Fluid Mech.*, **79**, 361-385, (1998).

[7] J. Bonvin, M. Picasso, and R. Stenberg, GLS and EVSS methods for a three-field Stokes problem arising from viscoelastic flows, *Comput. Meth. Appl. Mech. Engrg.*, **190**, 3893–3914, (2001).

[8] A. Fortin, R. Guenette, and R. Pierre, On the discrete EVSS method, *Comput. Meth. Appl. Mech. Engrg.,* **189**, 121–139, (2000).

[9] M. Fortin, R. Guenette, and R. Pierre, Numerical analysis of the modified EVSS method, *Comput. Meth. Appl. Mec. Engrg.,* **143**, 79–95, (1997).

[10] R. Guenette and M. Fortin, A new mixed finite element method for computing viscoelastic flows, *J. Non-Newtonian Fluid Mech.,* **60**, 27–52, (1995).

[11] J. Kwack, A. Masud, A three-field formulation for incompressible viscoelastic fluids, *Int. J. Eng. Sci.*, **48**, 1413-1432, (2010).

[12] J. G. Oldroyd, On the formulation of rheological equations of state, *Proc. R. Soc. London, Ser. A*, **200**, 523-541, (1950).

[13] H. Giesekus, A simple constitutive equation for polymer fluids based on the concept of deformation-dependent tensorial mobility, *J. Non-Newtonian Fluid Mech.*, 11, 69-109, (1982).

[14] N. Phan-Thien, A nonlinear network viscoelastic model, *J. Rheol.*, **22**, 259, (1987).

[15] J. G. Heywood, R. Rannacher, S. Turek, Artificial boundaries and flux and pressure conditions for the incompressible navier–stokes equations, *Int. J. Num. Meth. Fluid.*, **5**, 325-352, (1996).

[16] P. Westervoß, The Tensor Diffusion approach as a novel technique for simulating viscoelastic fluid flows, *Ph.D. thesis, TU Dortmund*, (2021).

[17] V. Girault and P. A. Raviart, Finite Element Methods for Navier-Stokes equations, *Springer*, (1986).

[18] Fortin, M. and Pierre, R. On the convergence of the mixed method of Crochet and Marchal for viscoelastic flows, *Comp. Meth. in App. Mech. and Eng.*, **73**, 341–350, (1989).

[19] M. Fortin and A. Fortin, A new approach for the FEM simulation of viscoelastic flows, *J. Non-Newtonian Fluid Mech.*, **32**, 295–310, (1989).

[20] J. Marchal, M. Crochet, A new mixed finite element for calculating viscoelas- tic flow, *J. Non-Newtonian Fluid Mech.*, **26**, 77-114, (1987).

[21] S. Turek and A. Ouazzi, Unified edge–oriented stabilization of nonconforming FEM for incompressible flow problems: Numerical investigations, *J. of Num. Math.*, **15**, 299–322, (2007).

[22] R. Keunings, On the high Weissenberg number problem, *J. Non-Newtonian Fluid Mech.*, **20** 209-226, (1986).

[23] R. A. Brown, R. C. Armstrong, A. N. Baris and P. W. Yeh, Galerkin finite element analysis of complex viscoelastic flows, *Comp. Meth. App. Mech. and Eng.*, **58**, 201-226, (1986).

[24] L. L. Ferrás, J. M. Nóbrega, F. T. Pinho, Analytical solutions for channel flows of phan-thien–tanner and giesekus fluids under slip, *J. Non-Newtonian Fluid Mech.*, **171-172**, 97-105, (2012).